Flights in a pseudo-chaotic system

J. H. Lowenstein[1] and F. Vivaldi[2]
[1]*Department of Physics, New York University, 2 Washington Place, New York, New York 10003, USA*
[2]*School of Mathematical Sciences, Queen Mary, University of London, London E1 4NS, United Kingdom*

(Received 31 March 2011; accepted 25 July 2011; published online 30 August 2011)

We consider the problem of transport in a one-parameter family of piecewise rotations of the torus, for rotation number approaching 1/4. This is a zero-entropy system which in this limit exhibits a divided phase space, with island chains immersed in a "pseudo-chaotic" region. We identify a novel mechanism for long-range transport, namely the adiabatic destruction of accelerator-mode islands. This process originates from the approximate translational invariance of the phase space and leads to long flights of linear motion, for a significant measure of initial conditions. We show that the asymptotic probability distribution of the flight lengths is determined by the geometric properties of a partition of the accelerator-mode island associated with the flight. We establish the existence of flights travelling distances of order $O(1)$ in phase space. We provide evidence for the existence of a scattering process that connects flights travelling in opposite directions. © *2011 American Institute of Physics*. [doi:10.1063/1.3624797]

The problem of transport is fundamental in dynamical systems theory and its applications. In the simplest scenario—much studied over several decades—one finds diffusive (Gaussian) collective transport, originating from exponentially unstable individual orbits. If the rate of exponential instability is not bounded away from zero, anomalous (non-diffusive) transport phenomena have long been known to exist. Such transport anomalies often feature so-called "flights," segments of orbits during which a particle proceeds at constant speed. The probability of a flight invariably decreases as an inverse power of the flight's length; this power is determined by the detailed structure of the complicated boundary between regular and chaotic regions in phase space. A complete theory of these transport anomalies is still missing. There is a class of non-smooth dynamical systems—of increasing importance in applications—which do not have exponential instability at all, but which nonetheless exhibit the kind of orbital complexity found at the boundary of chaos. Transport in these systems is typically anomalous. In this work, we investigate a two-dimensional area-preserving model of this type, obtained by combining two distinct isometries (rotations and translations). We show that the appearance of a slow variation of some local parameters across phase space increases dramatically the probability of occurrence of long flights. We compute such a probability, using geometrical methods.

I. INTRODUCTION

This paper is devoted to the study of transport in a two-dimensional area-preserving map, with "pseudo-chaotic" behaviour, continuing the work in Ref. 17. The suggestive—yet informal—term *pseudo-chaos*, was first used in the physics literature to characterise the statistical behaviour of dynamical systems with discrete energy spectrum.[7] This term now describes a broad range of complex dynamical phenomena that occur in systems with zero entropy, where chaos—positive Lyapounov exponent—is absent, but where a form of (non-exponential) sensitive dependence on initial conditions is still present.

An interesting example of anomalous transport, originating from accelerator-mode related flights, was studied in depth by Zaslavsky, Edelman, and Niyazov[19,20] in the web map with 4-fold rotational symmetry, with the translational symmetry of a simple square lattice. The authors found that for special parameter values, the chaotic sea of the fundamental square contains small accelerator-mode islands surrounded by self-similar island-chain hierarchies which are responsible for lengthy flights and super-diffusive asymptotic behaviour on the infinite plane. Similar effects were found in the lifted standard map,[19] as well as for the Cassini billiard (particle scattering elastically from a square lattice of Cassini ovals).[18] A somewhat different mechanism, but again associated with accelerator modes, was found by Dana[9] in the context of a web map with 3-fold symmetry. We note that the connection between anomalies in transport processes and the presence of stable islands in a chaotic sea has been known for a long time [Ref. 6, Sec. 5.5].

Pseudo-chaos is ubiquitous in *piecewise isometric systems*. These are higher-dimensional generalisations of interval-exchange maps, in which the dynamics is locally a translation, rotation, or reflection. The local isometric domains are called *atoms*, and the map acts discontinuously at the boundary of the atoms. Interesting asymptotic phenomena take place in the so called *exceptional set* (the closure of the set of points whose orbits get arbitrarily close to the discontinuity of the map), which plays the same role as the set of separatrices in smooth maps. In recent years these systems have attracted much attention, in both theory and applications (see Refs. 1, 8, 10, 17, and references therein). Piecewise isometries have zero topological entropy.[5,12] Nonetheless, their behaviour can be exceedingly complex, and very few general results are available. For instance, the

extent to which the exceptional set can exhibit mixing is not known. (There is no higher-dimensional analogue of the Avila-Forni theorem,[3] which states that almost every interval-exchange transformation is weak-mixing.) The question of the positivity of the measure of the exceptional set—known as Ashwin's conjecture[2]—also remains unresolved. (For a recent development, see Ref. 13.)

Transport phenomena in piecewise isometries remain largely unexplored. In Ref. 16, a family of kicked-oscillator models was introduced, leading to a skew system, namely a two-dimensional lattice map driven by a piecewise isometry of the torus. It was shown that the orbits in the exceptional set of the piecewise isometry can generate non-trivial lattice motions, featuring various types of anomalous transport. In particular, for a specific choice of parameters (corresponding to a rational rotation studied in Refs. 1 and 14), the existence of super-diffusion was demonstrated. In Ref. 11, a piecewise isometry of the plane was studied, consisting of a rotation followed by a piecewise translation. It was shown that almost all points are recurrent, even if Poincaré recurrence theorem does not apply because the system has an infinite invariant measure.

In the present paper we study flights in a one-parameter family of two-dimensional piecewise isometries. In this model, long flights are generated by a novel mechanism, namely the adiabatic destruction of accelerator-mode islands. We will show that while an accelerator mode islands always supports flights, its adiabatic destruction results in a substantial increase of the measure of initial conditions corresponding to flights.

We consider the following map F of the unit square $\Omega=[0,1)^2$

$$\begin{aligned} &F:\Omega\to\Omega \quad (x,y)\mapsto(\lambda x-y+\iota(x,y),x)\\ &\iota(x,y)=-\lfloor\lambda x-y\rfloor, \end{aligned} \tag{1}$$

where $\lfloor\cdot\rfloor$ denotes the floor function and $|\lambda|<2$. This map is area-preserving. It consists of a linear elliptic map $(x,y)\mapsto(\lambda x-y,x)$, followed by a piece-wise translation which brings the point back to the unit square Ω. The map F has time-reversal symmetry[15]

$$F^{-1}=G\circ F\circ G^{-1} \quad G:\Omega\to\Omega \qquad (x,y)\mapsto(y,x). \tag{2}$$

It is linearly conjugate to a piecewise rotation on a rhombus with rotation number ρ, where $\lambda=2\cos(2\pi\rho)$. Depending on the value of λ, this map has two or three atoms.

We are interested in the limit $\lambda\to 0$, some properties of which were studied in Ref. 17. At $\lambda=0$, the dynamics is trivial, a rotation by $\pi/2$. As λ approaches 0, the phase space decomposes into two parts, a central disc supporting regular motions (rotation by an angle approaching $\pi/2$), and four corner sectors with highly non-trivial dynamics(see Figure 1). The corner sectors feature infinitely many islands, immersed in a region with very complicated features. Because in this limit the phase space becomes very homogeneous, the study of some aspects of transport outside the aforementioned islands becomes possible. This justifies our interest in this limit.

In Ref. 17, it was shown that the dynamics outside the central disc may be studied via the return map L of a certain domain Λ, a thin strip of length $O(1)$ and thickness $O(\lambda)$

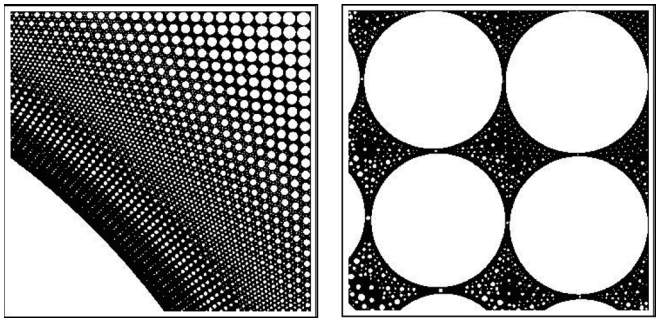

FIG. 1. Left: Detail of the phase portrait of the map F for $\lambda=10^{-2}$, corresponding to an irrational value of the rotation number ρ, close to $1/4$. A portion of the large central island appears in the SW corner of the picture. Right: Magnified view of the region near the NE corner.

located within one of the corner sectors of Figure 1. As $\lambda\to 0$, the domain Λ, rescaled in such a way as to have thickness $O(1)$, becomes an infinite strip; its return map is a piecewise isometry with infinitely many atoms (see Figure 5). Within each atom there is a single symmetric elliptic fixed point, surrounded by an island of maximal size, which corresponds to an elliptic periodic orbit of the original map F. These are the *primary islands*. Even though the difference between adjacent atoms becomes negligible in the limit, the strip Λ is not translationally invariant. As a consequence, the location and size of the islands changes slowly with the position along the strip, and so do the features of the complementary region. The main result concerning the primary islands of the map F is that, as $\lambda\to 0$, the decrease in the size of the islands balances exactly the increase of their number, so that the islands' total measure approaches a positive limit [Ref. 17, Theorem A].

The purpose of this paper is to analyse an important aspect of the dynamics outside the primary islands, namely the existence of flights with lengths of order $O(1)$ for orbits occupying a substantial measure. Their presence establishes the piecewise connectedness of this region, because an isolating invariant set cannot exist on a flight's path. We describe in detail the geometrical structure that determines the probability distribution of the flights' lengths. The asymptotic aspects of these dynamics depend on the structure of the exceptional set within the complement of the primary islands, the so-called *pseudo-chaotic domain*. This research aims to shed some light on the structure of this domain, whose properties are little known.

We first review the model in Ref. 17, and the associated map L of the domain Λ (Sec. II). Numerical experiments reveal the presence of intermittent behaviour, with flights along Λ separated by bursts of pseudo-chaotic behaviour. To explain these phenomena, we define simplified models, which introduce gradually the full complexity of the map L, isolating important dynamical features (Sec. III). The simplest model—the *local model*—consists of an infinite array of identical piecewise isometries with two atoms (Figure 6). The local model allows us to explore the region outside the primary islands in the limit $\lambda\to 0$ (which was not considered in Ref. 17), revealing a very rich dynamics. In the local representation, the domain Λ is an infinite strip; using translational invariance, we obtain a six-atom piecewise isometry of the two-dimensional torus (Figure 7). Every periodic

island on the torus which does not lift to a periodic island on the strip becomes an *accelerator mode*, resulting in sets of positive measure travelling to infinity at constant speed, in both directions. In the immediate vicinity of an accelerator mode island, orbits exist which remain attached to it for a long, but finite, number of iterations. These are the *flights*.

Due to spatial inhomogeneity, the size and location of the islands of the map L change adiabatically as one proceeds along the chain of atoms. To reproduce this phenomenon, we introduce a slow spatial modulation of the parameters of the local model. The resulting *periodic chain model* (Figure 8), which we study in Sec. III B, also has translational invariance, but the period comprises a long chain of atoms. This period is adjusted so as to match the geometric parameters of the original map F.

All models analysed in this paper admit explicit representations of their geometric structure in terms of rational functions of the parameters. We exploit this feature in order to derive exact and asymptotic expressions of all relevant dynamical quantities, using computer algebra.

In Sec. IV, we study transport. We begin by analysing the accelerator islands of the local map (Sec. IV A), and the flight generation near the boundary of such islands (Sec. IV B). We then show that the slow parametric modulation of the periodic chain map converts the interior of the accelerator islands into families of flights. We construct a partition of the islands which corresponds to flights of different length, thereby determining the measure of orbits comprising flights of a given length. In particular, we show that flights exist which propagate through half the spatial period of the periodic chain model (Sec. IV C). By comparing the asymptotic properties of the original map with those of the periodic chain model, we show that the former supports flights of length $O(1)$ (Sec. IV D).

Finally, in Sec. IV E, we briefly consider the dynamical processes that join flights together. We demonstrate experimentally the existence of a scattering mechanism which connects a flight to its twin moving in the opposite direction.

Some formulae are provided in Appendix.

II. STRUCTURE OF PHASE SPACE

We briefly review the main constructions in Ref. 17. When λ is close to zero, the map F approaches a rotation by $\pi/2$ (Figure 2), and has two atoms, one of which is of area $O(\lambda)$. The square, Ω, is partitioned into an invariant central disc (the maximal disc of the larger atom), and four corner sectors, where the dynamics of interest to us takes place. Let Σ denote the North-East sector. In the following, we will often use compass directions, NW, SE, etc., to denote the upper-left, lower-right, etc., corners of quadrilaterals. The mismatch between the action of F and a rotation by $\pi/2$ causes the first few images of the discontinuity set (the boundary of the atoms of F) to form a regular net of segments, which envelop the central disc. The distance between adjacent segments in the net is $O(\lambda)$, so that the sector Σ is subdivided into quadrilaterals of area $O(\lambda^2)$.

Over the sector Σ, the iterated map F (Ref. 4) is close to the identity, and it can be shown that all orbits leaving Σ eventually return to it, apart, possibly, from a set of measure

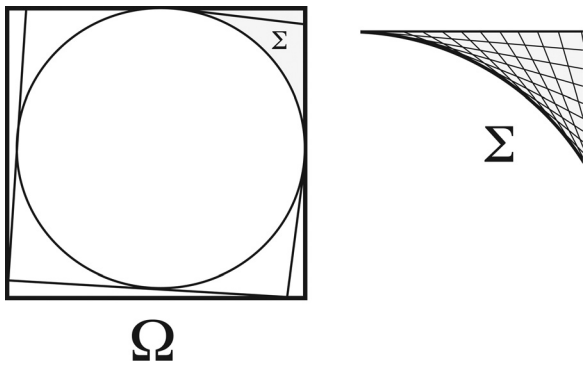

FIG. 2. Left: Mismatch between the action of F on Ω and a rotation by $\pi/2$, for a parameter value close to zero. Shown are the first few images of the boundary of Ω, which are tangent to the central island. Right: Dominant features of the discontinuity set in the North-East sector Σ.

$O(\lambda^3)$. The top row of quadrilaterals in Σ forms a thin strip Λ, which serves as surface of section for the orbits outside the central disc. The return map L of Λ is the composition of two involutions [Ref. 17, Theorem A]

$$L = H \circ G. \tag{3}$$

Each involution is conjugate to a piecewise isometry and the number of atoms goes to infinity as $\lambda \to 0$. Let the integers n and m label the atoms of G and H, respectively. Each atom is a quadrilateral (apart from a bounded number of exceptions), and the fixed set of the corresponding involution is a diagonal (Figure 5) [Ref. 17, Theorems 6 and 11]. These fixed sets intersect transversally, giving rise to a two-parameter family of symmetric fixed points, labelled by n and m. Each fixed point is surrounded by a disc of maximal size and the total area of these discs approaches a positive limit as $\lambda \to 0$ [Ref. 17, Theorem B].

We are interested in the dynamics of L in Λ, outside these islands, and for small values of λ. The vertices of the atoms of G and H are rational functions of λ, which can be computed explicitly [Ref. 17, Lemma 12]. From these formulae, one finds that the difference between adjacent atoms of G (corresponding to consecutive values of n) vanishes with λ, and so the system has an approximate translational invariance (see Figure 3).

We are led to consider the limiting case of exact translational invariance, represented by the *local model*, which corresponds to a piecewise isometry on the torus (see Sec. III A). By continuity, this map also has time-reversal symmetry. The spatial periodicity introduces a new family of periodic islands, whose lifting to the infinite strip are accelerator modes. These orbits are necessarily non-symmetrical, and they come in pairs travelling in opposite directions.

From the above considerations, one would expect the original model—seen as a perturbation of the local model—to support quasi-accelerator modes (flights), over a set of positive measure. This is indeed the case. In Figure 4, we

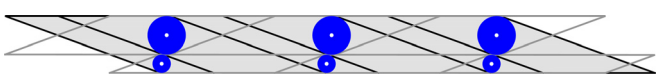

FIG. 3. (Color online) Atoms of the map L, for $\lambda = 10^{-4}$, showing a very nearly periodic environment. The discs are the primary islands in three adjacent atoms of G, corresponding to $n = 6099, 6100, 6101$.

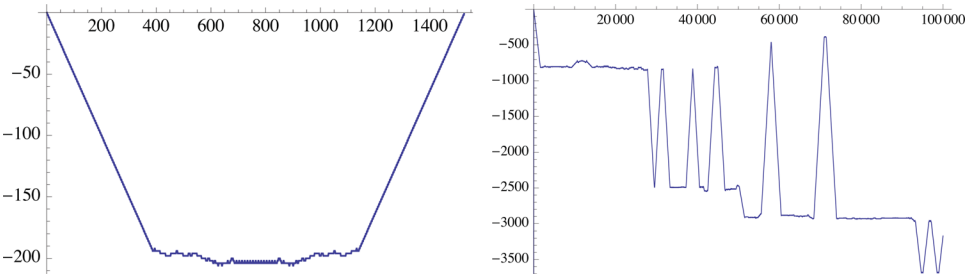

FIG. 4. (Color online) Flights of the map L, for $\lambda = 10^{-4}$. Left: A flight connected to its time-reversal twin. Right: A complex sequence of flights having the same speed.

plot the position along the chain (represented by the G-atom number n) as a function of time, for two orbits with initial condition chosen within accelerator modes of the local model. We observe the presence of flights, connected by motions with irregular features, but distinctively localised in space. The relation between the G-atom number and the actual position within the strip Λ depends on λ, as should be clear from Figure 2 (right). (See Sec. IV for details.)

In Sec. III, we will develop suitable models of the map L, which will be crucial to the analysis of flights to be carried out in Sec. IV.

III. SIMPLIFIED MODELS OF THE RETURN MAP

If we change coordinates so as to turn L into an actual piecewise isometry, each four-sided G-atom becomes a *kite*, namely a quadrilateral with reflection about one diagonal, the fixed set Fix G (see Figure 5). Now consider the boundary segment ∂H between the mth and the $(m+1)$th atoms of the involution H, for some m. (In the notation of Ref. 17 the vertices of ∂H are the points $P_0(m)$ and $P_1(m)$.)

We consider the chain of kites which intersect ∂H. This chain has a *central kite*, for which ∂H comes closest to the midpoint of Fix G (Figure 5). Up to an overall affine transformation fixing the position, orientation, and scale of the system on the plane, the geometry is determined by four parameters:

- g_0, where $a_0 = g_0 + 1/g_0$ is the length of the top side of the central kite,
- δ, the ratio of lengths a_0 and a_{-1} of the central kite's sides, minus 1,
- h_0, the ordinate of the intersection of ∂H with the vertical line going through the mid-point of Fix G in the central kite,
- ε, the slope of the segment ∂H, assumed to be smaller than the slope of the bottom edge of the kite.

In the original model, all parameters depend on λ, but for our purpose it is convenient to treat them as being independent.

Recalling that on each kite the map G acts as a reflection with respect to a diagonal, one can show by an inductive argument that the parameters θ and δ determine the shape of all kites. Likewise, the segment ∂H divides Λ into two domains, where H acts the reflection sending the top boundary to the bottom one. Thus h_0 and ϵ determine Fix H, and, again by induction, all the other atoms of H.

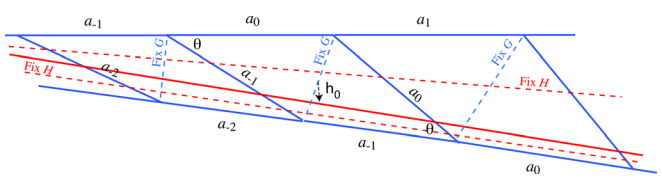

FIG. 5. (Color online) Atoms of a kite chain, including the central kite. Within each atom, the action of the map is a reflection G about Fix G, followed by a reflection H about the relevant branch of Fix H. The parameters are explained in the text, with $g_0 = \tan(\theta/2)$.

If Λ is infinite, then this construction will generate infinitely many kites. Otherwise some irregular atoms may appear near the right and left boundaries of Λ. In the original model, Λ is finite, and the rightmost G-kite is regular, meaning that its right side coincides with the boundary of Λ. (This constraint eliminates one parameter.) There are however irregular G-kites near the tip of Λ, and irregular H-kites at both ends.

We are interested in the case where the kite chains are of length $O(\lambda^{-1})$, where λ is very small. In such a case, three out of the four parameters, namely δ, h_0, and ϵ will also be small. By setting one or more of these to be exactly zero, we obtain simpler models which nevertheless capture the essential dynamical behaviour of the full model.

If $\delta = 0$, all kites become copies of a single rhombus, and the involution G is periodic. This allows for the possibility of introducing periodic boundary conditions on the chain. Indeed, setting one (but not both) of the other small parameters equal to zero, we obtain two significant periodic models, namely the *local model* L_{loc} with $\epsilon = 0$ (its period a is a single G-kite) and the *periodic chain model* L_{pc} with $h_0 = 0$ (its period b is an H-kite). Each periodic model merits our careful attention below.

A. Local map

The local map is obtained by setting $\delta = \epsilon = 0$ in the kite chain described in the above paragraph. This dynamical system describes the original map L in the $\lambda \to 0$ limit, and in the immediate vicinity of a given kite. Such a kite is identified by specifying the two remaining parameters g and h. In this section, we regard these parameters as being independent; their relation will be discussed in Sec. IV D.

In the local model, the (normalised) domain Λ becomes the horizontal strip $\Lambda = \{(x,y) \in \mathbb{R}^2 : -1 \le y < 1\}$, and the set ∂H is the line $y = h$. The involution H has two atoms. It simultaneously reflects vertically the pieces of Λ above and below the line $y = h$ (see Figure 6)

$$H : \Lambda \to \Lambda \quad (x,y) \mapsto \begin{cases} (x, -y + h + 1) & \text{if } y > h \\ (x, -y + h - 1) & \text{if } y \le h \end{cases}. \tag{4}$$

Clearly, H is invariant under all horizontal translations.

All kites of the involution G are identical and centrally symmetric. Placing the barycentre of the central kite Π at the

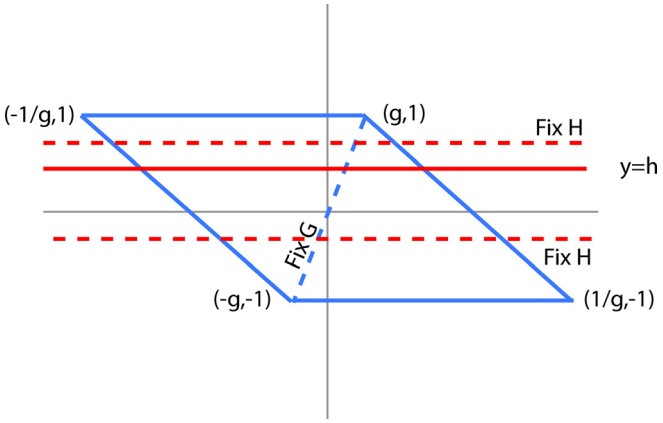

FIG. 6. (Color online) An atom of the local map L_{loc}. The dashed lines are the fixed lines of the involutions G and H.

origin, we obtain a rhombus, which we represent as a list of vertices, ordered clockwise. We find

$$\Pi = [(-1/g, 1), (g, 1), (1/g, -1), (-g, -1)],$$

where $g = \tan(\theta/2)$ (recall that θ is the (positive) angle of the NW and SE vertices of Π, see Figure 5). We stipulate that Π contains its bottom and left sides, including the vertex $(-g, -1)$, and no other part of its boundary.

The parallelogram Π tiles Λ under the translation T, where

$$T : \Lambda \to \Lambda \quad (x, y) \mapsto (x + a, y) \quad a = g + \frac{1}{g}. \tag{5}$$

The action of G on Π is a reflection with respect to its SW-NE diagonal. We find

$$G : \Pi \to \Pi \quad (x, y) \mapsto (2x' - x, 2y' - y), \tag{6}$$

where

$$x' = \frac{g}{g^2 + 1}(gx + y) \quad y' = \frac{1}{g}x'. \tag{7}$$

The map G extends by translation to all copies of the central rhombus Π, thereby defining an isometric involution of Λ.

The local map L_{loc} is defined as the composition of the above involutions: $L_{\mathrm{loc}} = H \circ G$. The atoms of L_{loc} on the central rhombus Π are given by

$$\Pi_0 = [(-1/g, 1), (a(h-c)/2, 1), (a(h+c)/2, -1), (-g, -1)], \tag{8}$$

$$\Pi_1 = [(a(h-c)/2, 1), (g, 1), (1/g, -1), (a(h+c)/2, -1)]. \tag{9}$$

By construction, the local map commutes with the horizontal translation T by a, so we define the translated copies of the rhombus Π and its atoms

$$\Pi^{(n)} = T^n(\Pi) \quad \Pi_i^{(n)} = T^n(\Pi_i) \quad n \in \mathbb{N} \quad i = 0, 1. \tag{10}$$

To obtain an explicit expression for L_{loc}, we define

$$c = \frac{1 - g^2}{1 + g^2} \quad s = \frac{2g}{1 + g^2} = \frac{2}{a}. \tag{11}$$

(Note that $c = \cos(\theta)$ and $s = \sin(\theta)$, where θ is the acute vertex angle of the central kite.) We obtain

$$L_{\mathrm{loc}}(z) = T^n(J \cdot T^{-n}(z) + \delta_i), \quad z \in \Pi_i^{(n)}, \quad n \in \mathbb{N} \quad i = 0, 1, \tag{12}$$

where

$$J = \begin{pmatrix} -c & s \\ -s & -c \end{pmatrix}, \quad \delta_i = (0, 2i + h - 1).$$

The matrix J has unit determinant and complex eigenvalues. It represents a clockwise rotation by an angle $2\pi\rho$, where

$$\rho = \frac{1}{2\pi}\arccos\left(\frac{g^2 - 1}{g^2 + 1}\right).$$

The map L_{loc} has two symmetric fixed points, one in each atom, lying at the intersection of Fix G and Fix H (Figure 6). From translational invariance, we obtain infinitely many symmetric fixed points, which are the local images of the primary periodic points studied in Ref. 17, located in a small neighbourhood of a point in Λ. The correspondence between the parameter λ, n, and m of the map L and the parameters g and h of the local map L_{loc} is given by the following formulae:

$$g = \tau + O(\lambda) \quad h = \frac{1}{\tau} + 2m + O(\lambda), \tag{13}$$

where

$$\tau = \tan\left(\frac{\pi}{4} - 2n\arcsin\left(\frac{\lambda}{2}\right)\right) = \tan\left(\frac{\pi}{4} - n\lambda\right) + O(\lambda^2). \tag{14}$$

Since L_{loc} commutes with the translation T, it can be reduced to a piecewise isometry $\overline{L}_{\mathrm{loc}}$ of the torus, obtained from Π by identifying the sloping edges. Due to the added periodicity, each atom of L_{loc} splits into three atoms of $\overline{L}_{\mathrm{loc}}$. Indeed, the image of each atom Π_i intersects $L_{\mathrm{loc}}^k(\Pi)$, for $k = -1, 0, 1$. Accordingly, we let

$$\Pi_i = \Pi_{i,-1} \cup \Pi_{i,0} \cup \Pi_{i,1},$$

where

$$\Pi_{i,k} = \Pi_i \cap L_{\mathrm{loc}}^{-1}(T^k(\Pi)) \quad i = 0, 1, \quad k = -1, 0, 1. \tag{15}$$

The atoms $\Pi_{i,1}$ and $\Pi_{i,-1}$ are isosceles triangles, with base angles equal to θ, and they are adjacent, respectively, to the NW and SE vertices of the atom Π_i. The atoms $\Pi_{i,0}$ are hexagons (see Figure 7).

We obtain a six-atom piecewise isometry, mapping Π onto itself

$$\overline{L}_{\mathrm{loc}}(z) = J \cdot z + \delta_{i,k}, \quad z \in \Pi_{i,k}, \quad \delta_{i,k} = (-ka, 2i + h - 1).$$

Formulae for the atoms of $\overline{L}_{\mathrm{loc}}$, with explicit parameter dependence, are found in Appendix section "Local map: Atoms."

The fixed points of $\overline{L}_{\mathrm{loc}}$ lie in the intersection of the atoms with their images (see Figure 7). An explicit computation, using the expressions for $\overline{L}_{\mathrm{loc}}$ and $\Pi_{i,k}$ given above,

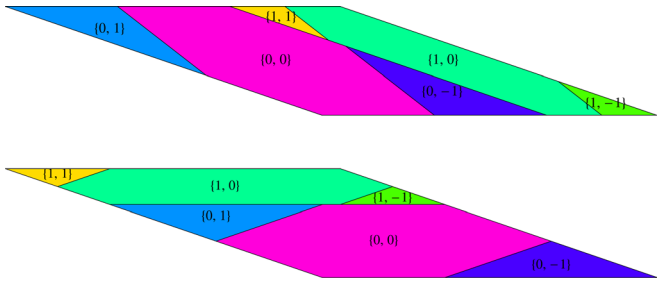

FIG. 7. (Color online) Top: Atoms of the local map $\bar{L}_{\rm loc}$ of the rhombus Π, for $g = 1/6$, $h = 171/500$. Bottom: Images of the atoms under the map.

shows that each atom $\Pi_{i,k}$ of $\bar{L}_{\rm loc}$ contains a fixed point, which exists in the parameter range specified below.

atom	parameters	symmetric?
$\Pi_{0,0}$	all	yes
$\Pi_{0,1}$	$h \geq g^2$	no
$\Pi_{0,-1}$	$h < -g^2$	no
$\Pi_{1,0}$	all	yes
$\Pi_{1,1}$	$h < -g^2$	no
$\Pi_{1,-1}$	$h \geq g^2$	no

(16)

The non-symmetric fixed points correspond to accelerator modes, see Sec. IV A.

B. Periodic chain map

The periodic chain (PC) map $L_{\rm pc}$ is obtained by setting $\delta = h_0 = 0$ in the kite chain described in Sec. III, but allowing the parameter ϵ to be different from zero. This dynamical system is an approximation of the original return map L in the $\lambda \to 0$ limit, over a spatial range of order $O(1)$ corresponding to a single m-value. Once again, the map is a composition of two time-reversing involutions, G and H, but now the arrays of atoms of G and H are endowed with commensurate periodicities, a and b. In addition, we will find related involutions G' and H' with restricted, but still useful, time-reversing properties.

The periodic chain map is a chain of N identical rhombi, repeating indefinitely along the strip $\Lambda = \{(x, y): -1 \leq y < 1\}$. The rhombi, labelled by n, are arranged symmetrically around a central rhombus, corresponding to $n = 0$. Hence, N is an odd integer. The spatial periodicity of the periodic chain map $L_{\rm pc}$ is $b = Na$, where $a = g + 1/g$ is the periodicity of the local map $L_{\rm loc}$. The atoms of H are arranged in such a way as to extend over one period. The setup is illustrated in Figure 8, for one period. The slope ϵ of the H-atom boundary line ∂H is

$$\epsilon = \frac{2}{\sqrt{b^2 - 4}}. \tag{17}$$

In addition, we introduce the notation

$$\epsilon_1 = \sqrt{1 + \epsilon^2} = \frac{b\epsilon}{2}.$$

The periodic chain map decomposes as $L_{\rm pc} = H \circ G$ where the involutions G and H are given by

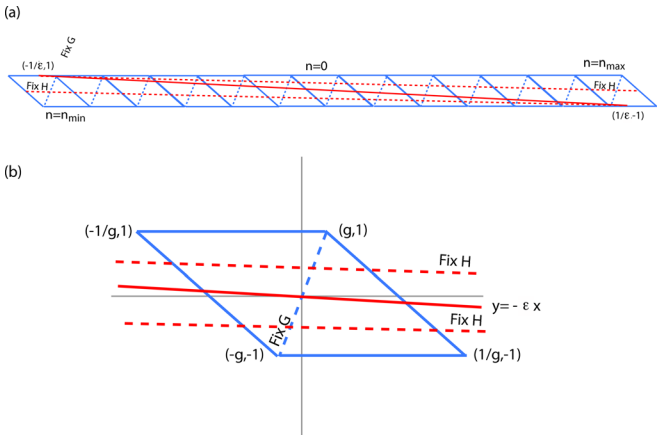

FIG. 8. (Color online) (a) Domains and fixed lines of the periodic chain map. (b) Detail for the central G-atom ($n = 0$).

$$G\begin{pmatrix} x \\ y \end{pmatrix} = \begin{pmatrix} na \\ 0 \end{pmatrix} + \begin{pmatrix} -c & s \\ s & c \end{pmatrix}\begin{pmatrix} x - na \\ y \end{pmatrix}, \tag{18}$$

$$H\begin{pmatrix} x \\ y \end{pmatrix} = \begin{pmatrix} (m - \frac{1}{2})b \\ 0 \end{pmatrix} - \frac{1}{\epsilon_1}\begin{pmatrix} -1 & \epsilon \\ \epsilon & 1 \end{pmatrix}\begin{pmatrix} x - (m - \frac{1}{2})b \\ y \end{pmatrix}, \tag{19}$$

with

$$m = m(x, y) = \left\lceil \frac{x + y/\epsilon}{b} \right\rceil. \tag{20}$$

The fixed lines of the involutions are

$$\mathrm{Fix}G = \{(x, y) : y = (x - na)/g,\ n \in \mathbb{Z}\},$$

$$\mathrm{Fix}H = \left\{(x, y) : y = \left(\frac{\epsilon_1 - 1}{\epsilon}\right)\left(x - \left(m - \frac{1}{2}\right)b\right),\ m \in \mathbb{Z}\right\}.$$

The atoms of H are the rhombi

$$\Psi^{(m)} = \Psi^{(0)} + (mb, 0) = \{(x, y) : m(x, y) = m\}, \quad m \in \mathbb{Z},$$

with m given by (20) and

$$\Psi^{(0)} = \left[\left(-\frac{1}{\epsilon} - b, 1\right), \left(-\frac{1}{\epsilon}, -1\right), \left(\frac{1}{\epsilon}, -1\right), \left(\frac{1}{\epsilon} - b, -1\right)\right],$$

with vertices arranged clockwise. Note that the total horizontal extent of each atom is $\sqrt{b^2 - 4} + b$, slightly less than two full periods of the chain for large N.

The map $L_{\rm pc}$ is piecewise a composition of two reflections. Hence it is a piecewise isometry, given by

$$L_{\rm pc}(z) = J \cdot z + \delta_{i,n}, \quad z \in \Pi_{i,n}, \quad i = 0, 1,$$

where the rotational part is

$$J = \begin{pmatrix} c_1 & s_1 \\ -s_1 & c_1 \end{pmatrix}, \quad c_1 = \frac{-c - \epsilon s}{\epsilon_1}, \quad s_1 = \frac{s - \epsilon c}{\epsilon_1}, \tag{21}$$

and the translations are

$$\delta_{i,n} = \frac{na}{\epsilon_1}(1 - c_1\epsilon_1, -\epsilon + s_1\epsilon_1) + \left(2\left\lfloor \frac{2n + N - 1}{2N} \right\rfloor + 2i - 1\right)\left(\frac{\epsilon_1 - 1}{\epsilon}, 1\right).$$

The atoms $\Pi_i^{(n)}$ are given explicitly in Appendix section "Periodic chain map: Atoms."

In addition to the pair of time-reversing involutions G and H, the periodic chain model possesses a related pair of involutions, G' and H', which provide a restricted form of time-reversal symmetry. This will turn out to be especially relevant to the analysis of long flights in Sec. IV C. The map H' is defined as a reflection about the *short* diagonal of each H-atom $\Psi^{(m)}$. Specifically,

$$H'\begin{pmatrix} x \\ y \end{pmatrix} = \begin{pmatrix} (m-\frac{1}{2})b \\ 0 \end{pmatrix} + \frac{1}{\epsilon_1}\begin{pmatrix} -1 & \epsilon \\ \epsilon & 1 \end{pmatrix}\begin{pmatrix} x-(m-\frac{1}{2})b \\ y \end{pmatrix},$$

with m given by Eq. (20). The following result establishes the significance of H' for the periodic chain map L_{pc}:

Lemma 1: Let $B^{(m,n)}$ be the interior of the convex polygon $\Pi_i^{(n)} \cap G(\Pi_i^{(n)})$, where

$$i = i(m,n) = \begin{cases} 0 & \text{if} \quad n_0 + mb \le n < n_0 + (m+1)b \\ 1 & \text{if} \quad n_0 + (m-1)b \le n < n_0 + mb. \end{cases}$$

Then, on the set $\cup_{m,n} B^{(m,n)}$, the following identity holds

$$L_{\mathrm{pc}} = H' \circ L_{\mathrm{pc}}^{-1} \circ H'.$$

Proof: By periodicity, it will be sufficient to restrict ourselves to the H-atom $\Psi^{(0)}$ and the $\Pi^{(n)}$ which intersect it. The vertices of the polygons $B^{(0,n)}$ can be computed explicitly using the formula (18) for G and the formulae for the atoms $\Pi_i^{(n)}$ given in Appendix section "Periodic chain map: Atoms." The verification of the validity of the lemma from these formulae is a straightforward exercise in computer-assisted algebra.

In Sec. IV C below, we will see that the set $\cup_n B^{m,n}$ contains the pathways of all of the maximum-velocity flights in $\Psi^{(m)}$, apart from those on the discontinuity set, and so H' serves as an important reversal symmetry for such orbits. From the lemma, we can define a partner involution $G' = L_{\mathrm{pc}} \circ H'$ so that $L_{\mathrm{pc}} = H' \circ G'$ on $\cup_{m,n} B^{(m,n)}$. Note that G' maps $B^{(n_0+t)}$ into $B^{(n_0-t-1)}$, and consists of a reflection of each G-atom about its long diagonal, followed by an n-shift.

To each G-atom of the periodic chain map, identified by an integer n, we associate a pair g, h of parameters of the local map. Since all G-atoms are identical, the value of g is the same as that of the periodic chain map (determined by the central kite, see Figure 8), while h is given, in the central H-atom, by

$$h = -n\epsilon a, \tag{22}$$

where the parameters a and ϵ were defined in Eqs. (5) and (17), respectively. Geometrically, na gives the centre of the nth rhombus, while h is the vertical distance between the centre and the line ∂H.

The parameters of the periodic chain map are related to those of the original map as follows. We begin by fixing a value of m. This gives us N, which is the number of G-atoms intersecting the boundary between the mth and the $(m+1)$ atoms of H. To compute g, we identify the central kite, and then scale it until the mid-point of its lower side is at distance 2 from the line through the top side. This fixes the length of the top side. There is only one rhombus Π whose lower side belongs to the horizontal line going through this mid-point. This rhombus Π defines the value of g uniquely.

IV. TRANSPORT

In this section, we begin the study of transport along the strip Λ, which takes place in the complement of the primary islands. The simplest scenario is that of the local map L_{loc}, where transport is dominated by accelerator modes. The local map will serve as a template for the analysis of transport in the periodic chain map L_{pc}, which may be considered as an adiabatic perturbation of the local map. The periodic chain map is in turn a template for the original map L, where the translational invariance of the former is broken by a small asymmetry.

A. Accelerator modes

We consider the local map L_{loc}, developed in Sec. III A. The periodic points of its reduction $\overline{L}_{\mathrm{loc}}$ to the torus Π may be divided into two families, namely those which are also periodic under L_{loc}, and those which are not. The latter are *accelerator modes* of L_{loc}, namely orbits that have a non-zero (average) velocity v along Λ. More precisely, for every $z \in \Lambda$, we define

$$v(z) = \lim_{t\to\infty} \frac{L_{\mathrm{loc}}^t(z)}{t}, \tag{23}$$

if the limit exists. Thus z is an accelerator mode if $v(z)$ in non-zero. Clearly, $v(z)$ is the same for all points of the cell containing z. If z is a periodic point of $\overline{L}_{\mathrm{loc}}$, then $z = T^{-m}\left(L_{\mathrm{loc}}^n(z)\right)$, for some $m, n \in \mathbb{Z}$ with $n > 0$, and, therefore, $v(z) = am/n$. Because the parallelogram Π is equilateral, it is easy to see that

$$|v(z)| \le a, \tag{24}$$

where the maximal velocity corresponds, on average, to incrementing n by one at each iteration.

Accelerator modes, as defined via Eq. (23), are not necessarily periodic orbits of the reduced map. However, in the literature this term invariably refers to a (stable) periodic orbit, and in the present paper we shall also restrict our attention to the periodic case. A periodic accelerator mode is non-symmetric, because L_{loc} is conjugate to its inverse under G, and G sends an accelerator mode moving to the right into one moving to the left, which is a distinct orbit. For this reason, it suffices to consider accelerator modes with positive velocity.

We will concentrate on the case of maximal velocity a. To this end, we consider the fixed points of $\overline{L}_{\mathrm{loc}}$, classified in Eq. (16). By construction, the action of L_{loc} translates the fixed point in $\Pi_{i,k}$ by ka. Hence, only the value $k = 0$ leads to fixed points of L_{loc}, which correspond to the primary fixed points of the original map L. The other four fixed points are accelerator modes of maximal velocity. Let $z_i = (x_{i,1}, y_{i,1})$ be the accelerator fixed point located within $\Pi_{i,1}$, and let $\mathcal{A}_i$ be the corresponding cell. We have (for $g > 0$)

$$x_{i,1} = -\frac{g^2+1}{2} - \frac{h+2i-1}{2}, \tag{25}$$

$$y_{i,1} = -\frac{g^2+1}{2g} + \frac{h+2i-1}{2}. \tag{26}$$

The fixed point in $\Pi_{i,-1}$ is obtained from the above by changing sign.

Next we show that the islands $\mathcal{A}_i$ exhaust the set $\mathcal{A}$ of accelerator modes of maximal velocity, that is, every $z \in \mathcal{A}$ has a symbolic itinerary ((*i*, 1), (*i*, 1), (*i*, 1),…), visiting in succession the atoms $\Pi_{i,1}$, $T(\Pi_{i,1})$, $T^2(\Pi_{i,1})$,…. To see this, consider the sets

$$\Xi_{i,j} = \Pi_{j,1} \cap T^{-1}(L_{\rm loc}(\Pi_{i,1})) = \Pi_{j,1} \cap L_{\rm loc}(T^{-1}(\Pi_{i,1})), \quad i,j \in \{0,1\}.$$

This is the set of points in $\Pi_{i,1}$ whose image is in the atom $\Pi_{j,1}$ of the neighbouring rhombus, corresponding to successive code elements (*i*, 1) and (*j*, 1) in the symbolic itinerary. A straightforward calculation shows that for $h \geq g^2$,

$$z_0 \in \mathcal{A}_0 \subset \Xi_{0,0}, \quad \Xi_{0,1} = \Xi_{1,1} = \emptyset, \tag{27}$$

and for $h < -g^2$,

$$z_1 \in \mathcal{A}_1 \subset \Xi_{1,1}, \quad \Xi_{1,0} = \Xi_{0,0} = \emptyset. \tag{28}$$

From Eq. (27) it follows that for $h \geq g^2$, no periodic code can have the symbol (1, 1), and hence the only accelerator mode in the given parameter range is that with code ((0, 1), (0, 1),…), namely $\mathcal{A}_0$. The analogous argument for $h < -g^2$, with (0, 1) and (1, 1) interchanged, proves the uniqueness of $\mathcal{A}_1$.

The sets $\Xi_{0,0}$ and $\Xi_{1,1}$ are isosceles triangles for

$$g^2 < h < \frac{1+5g^2}{3-g^2} \quad \text{and} \quad -\frac{1+5g^2}{3-g^2} < h < -g^2, \tag{29}$$

respectively, and are quadrilaterals otherwise.

A straightforward calculation shows that the point z_i is equidistant from three sides of $\Xi_{i,i}$, and that the nearest points are mapped into each other by $L_{\rm loc}$. Thus the cell $\mathcal{A}_i$ is maximal. For irrational rotation number (see below), the distance from z_i to the boundary of Δ_i is the radius of $\mathcal{A}_i$, which is given by

$$r_i = \frac{1}{2}(|h| - g^2). \tag{30}$$

The island $\mathcal{A}_i$ has rotation number

$$\rho_i = \frac{1}{2\pi}\arccos\left(\frac{1-g^2}{1+g^2}\right). \tag{31}$$

B. Flight generation in the local model

In this section, we study an iterative process which generates flights in a "halo" region surrounding accelerator islands in the local model. By definition, a flight of length *t* maintains the same symbolic itinerary as the accelerator mode, for *t* iterations of $L_{\rm loc}$. In Sec. IV C, we will show how a small perturbation may convert the entire accelerator mode island $\mathcal{A}_i$ into flights, substantially increasing the measure of initial conditions that participate in this process. The parameters z_i, r_i and ρ_i of the island $\mathcal{A}_i$ will be important in this analysis.

We limit our discussion to the halo of the maximal velocity accelerator island ($v = a$). This case displays in their simplest form the features of trapping around more general accelerator islands. For any integer *n*, let $\Pi^{(n)} = T^n(\Pi)$ be the translated rhombus, and let

$$\Pi_i^{(n)} = T^n(\Pi_i), \quad \mathcal{A}_i^{(n)} = T^n(\mathcal{A}_i) \quad i = 0,1$$

be the corresponding atoms of $L_{\rm loc}$ and accelerator islands of maximal velocity, respectively. Furthermore, let

$$\Delta_0^{(n)} = L_{\rm loc}(\Pi_0^{(n-1)}) \cap \Pi_0^{(n)},$$

where the action of $L_{\rm loc}$ on the atom $\Pi_0^{(n-1)}$ is given by Eq. (12). The starting point of our flight-generating process is the polygon $\Xi^{(0)} = \Delta_0^{(0)}$. An important property of $\Delta_0^{(0)}$ is that it contains the accelerator mode island $\mathcal{A}_0^{(0)}$, with two of its edges tangent to $\mathcal{A}_0^{(0)}$. One of these edges lies along the cell boundary $\partial\Pi^{(n)}$, the other along the line $y = h$.

We now proceed to the first step of the iterative process. Since $\Xi^{(0)} \subset \Pi_0^{(0)}$, we can map it forward with $L_{\rm loc}$, defining

$$\Xi^{(1)} = L_{\rm loc}(\Xi^{(0)}) \cap \Pi_0^{(1)}, \quad \mathcal{W}^{(1)} = L_{\rm loc}(\Xi^{(0)}) \setminus \Xi^{(1)}.$$

Given that $L_{\rm loc}(A_0^{(0)}) = A_0^{(1)}$, it is easy to see that

$$\mathcal{A}_0^{(1)} \subset \Xi^{(1)} \subset \Delta_0^{(1)}, \quad \mathcal{W}^{(1)} \subset \Pi^{(0)}.$$

We note that, because $L_{\rm loc}$ is an isometry on each atom, the disk $\mathcal{A}_0^{(1)}$ will be tangent to two edges of $\Xi^{(1)}$, and if the rotation angle is incommensurate with 2π, neither of these edges lies along $\partial\Pi^{(1)}$. However, the disk is also tangent to the edge of $\Delta^{(1)}$ lying along $\partial\Pi^{(1)}$, and so we have three tangent edges.

It is clear that the step describing the construction, starting with $\Xi^{(0)}$, of $\Xi^{(1)}$ and $\mathcal{W}^{(1)}$, can be iterated arbitrarily many times, obtaining, after *t* steps, polygons $\Xi^{(t)}$ and $\mathcal{W}^{(t)}$ such that

$$\mathcal{A}_0^{(t)} \subset \Xi^{(t)} \subset \Delta_0^{(t)}, \quad \mathcal{W}^{(t)} \subset \Pi^{(t-1)}, \tag{32}$$

with $\mathcal{A}_0^{(t)}$ tangent to $t+2$ edges of $\Xi^{(t)}$. Moreover, the sequence of sets

$$L_{\rm loc}^{-t}(\mathcal{W}^{(t)}) \quad t = 0,1,\ldots$$

with $L_{\rm loc}^{-t}$ implemented by the isometry $L_0^{(0)-1} \circ \cdots \circ L_0^{(t-1)-1}$, forms a countable tiling of the halo region $\Xi^{(0)} \setminus \mathcal{A}_0^{(0)}$, with the *t*th tile constituting the initial domain of flights of length *t* for $t > 0$. The first 8 steps of the process described above are illustrated in Fig. 9. The resulting partition of the halo is exhibited in Fig. 10.

C. Flight generation in the periodic chain model

If we compare the phase portraits of respective rhombi of the local and PC maps with the same values of *g* and *h* (in the PC model, *h* is defined in Eq. (22)), we find a striking similarity everywhere except for the accelerator islands and their halos. In the PC model, the accelerator islands are absent, the corresponding region being replaced by spirals of

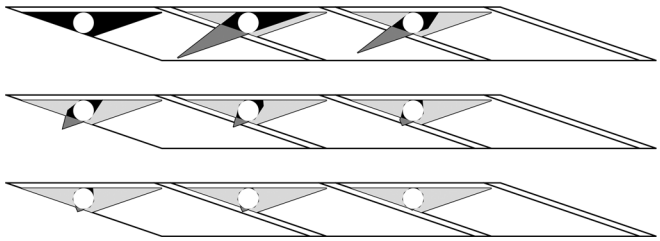

FIG. 9. First 8 steps of the iterative process described in the text, for the local map with $g=1/6$, $h=4/5$. The triangles $\Delta_0^{(t)}$ are shown in light grey. The polygons $\Xi^{(t)}$ and $W^{(t)}$ generated at step t are coloured black and grey, respectively. Superposed on each $\Xi^{(t)}$ is the accelerator island $A^{(t)}$, in white.

small polygonal domains $\mathcal{V}^{(t)}$ which are embarkation sites for flights of length t. Thanks to the double periodicity of the model, the number of such domains is bounded above by the long period N.

The mechanism for flight generation in the PC model is essentially the same as in the local model, but without the constant-radius accelerator islands $\mathcal{A}_0^{(t)}$ bounding below the polygons $\Xi^{(t)}$. Setting $n=n_0+t+1$, with $0\le t\le -n_0-1$, we can define $\Xi^{(0)}=\Delta_0^{(n_0+1)}$ and $\Xi^{(t)}$ for larger t by means of the same iterative process described in Sec. IV B, replacing the map $L_{\rm loc}$ by $L_{\rm pc}$, and denoting by $L_i^{(n)}$ the restriction of $L_{\rm pc}$ to the atom $\Pi_i^{(n)}$. To provide a contracting polygonal bound for the successive $\Xi_0^{(t)}$, $t=0,1,\ldots$, we rely on the second-order intertwining polygon,

$$\begin{aligned}\Sigma_0^{(n)} &= L_{\rm pc}(\Delta_0^{(n-1)})\cap\Pi_0^{(n)}\\ &= L_0^{(n-1)}\circ L_0^{(n-2)}(\Pi_0^{(n-2)})\cap L_0^{(n-1)}(\Pi_0^{(n-1)})\cap\Pi_0^{(n)}.\end{aligned}$$

Using the expressions (34) for the atom vertices, one can obtain an exact formula for area of $\Sigma_0(n)$ as a function of g,ε, and $h=-n\varepsilon(g+g^{-1})$. As h decreases from unity, the polygon shifts from a quadrilateral to a triangle at a certain value. We find the transition point to be

$$\begin{aligned}h&=\frac{(g-\epsilon)(1-3g^2+3\epsilon g-\epsilon g^3)-\sqrt{1+\epsilon^2}(2g+2g^3-\epsilon+\epsilon g^4)}{3g-g^3-\epsilon+3\epsilon g^2}\\ &=\frac{1+5g^2}{3-g^2}+\frac{1-16g^2-3g^4-2g^6}{g(3-g^2)^2}\epsilon+O(\epsilon^2).\end{aligned}$$

The area of $\Sigma_0^{(n)}$ continues to decrease beyond that point as a quadratic function

$$\mathrm{Area}(\Sigma_0^{(n)})=c(g,\epsilon)(h-h_*)^2,$$

where the bifurcation point h^* is given by

$$h_*=\frac{(g-\epsilon)(\epsilon g+1-\sqrt{1+\epsilon^2})}{\epsilon+g(\sqrt{1+\epsilon^2}-1)}=g^2-\frac{3g+g^3}{2}\epsilon+O(\epsilon^2),$$

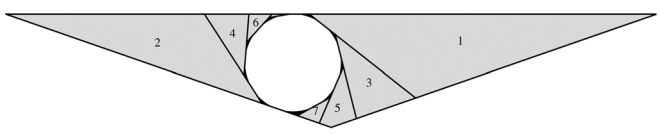

FIG. 10. Partition of $\Delta_0^{(0)}$ after 8 iterations. The numbered triangles are the images under $L_{\rm loc}^{-t}$ of the $\mathcal{W}^{(t)}$, and are the initial domains of the flights of length t, for $t=1,2,\ldots,8$. The accelerator island (grey disk) is inscribed in the decagon $L_{\rm loc}^{-8}(\Xi^{(8)})$, with all edges tangent.

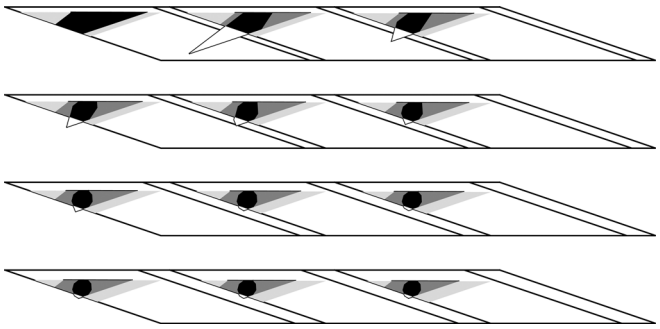

FIG. 11. First 11 steps of the iterative process described in the text, for the PC map with $g=1/6$, $N=100$, $n=-40,-39,\ldots,-29$. The intertwining domains $\Delta_0^{(n)}$ and $\Sigma_0^{(n)}$ are shown in light and dark grey, respectively. The polygons $\Xi^{(t)}$ and $W^{(t)}$ generated at step t are depicted in black and white, respectively.

while the coefficient function is

$$\begin{aligned}c(g,\epsilon)&=\frac{1-g^2+2\epsilon g+(2g^2-2\epsilon g+\epsilon^2g^2+\epsilon^2)(\sqrt{1+\epsilon^2}-1)/\epsilon^2}{\sqrt{1+\epsilon^2}(1-g^2+2\epsilon g)(2g-\epsilon+\epsilon g^2)}\\ &=\frac{1}{2g(1-g^2)}+\frac{(1-4g^2-g^4)}{4g^2(1-g^2)^2}\epsilon+O(\epsilon^2).\end{aligned}$$

For $g<1$ and ε sufficiently small, the bounding polygon $\Sigma_0^{(n)}$ contracts monotonically to a point, and the flight generation process proceeds up to its endpoint at

$$n_*=\left\lfloor -\frac{gh_*}{\epsilon(1+g^2)}\right\rfloor.$$

The flight generation process is illustrated in Figure 11. Here we have chosen g,N, and n for the initial cell to correspond to the local map parameters used in Figures 9 and 10.

The partition of $\Xi^{(0)}$ by the flight domains $\mathcal{V}^{(t)}=L_{\rm pc}^{-t}(\mathcal{W}^{(t)})$ for $n=n_0$ is shown in Figure 12.

Details of the forward spiral are given in Figure 13. Within $\mathcal{A}$ and the surrounding region, the tiles $\mathcal{W}^{(t)}$ spiral toward the centre of $\mathcal{A}$ while maintaining an approximately tangential orientation. These features are progressively distorted as one approaches the centre. The points in $\mathcal{W}^{(t)}$ travel from n_0 to n_0+t, increasing n by one unit at each step; then they are ejected from the accelerator mode (apart from finitely many exceptions, which may occur for small t). Thus the nearer to the centre is the initial condition, the longer is the flight.

The flight-induced destruction of the $h=1$ accelerator-mode island is graphically illustrated by plotting the area of the polygon $\Xi^{(t)}$ (what remains of the original $\Xi^{(0)}$ after t iterations of the map $L_{\rm pc}$). The decay curve for $g=1/6$, $N=1001$ is shown in Figure 14(a). Except very close to the endpoints, the area of $\Xi^{(t)}$ is always slightly larger than the

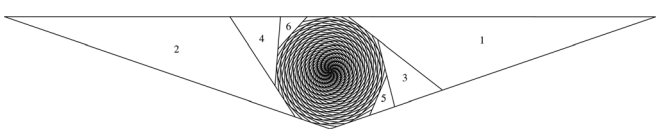

FIG. 12. Forward flight tiling of $\Delta^{(n_0)}$ for $g=1/6$, $N=1001$. The numbered domains $\mathcal{V}^{(t)}$ are the initial domains of the flights of length t, for $t=1,2,\ldots$.

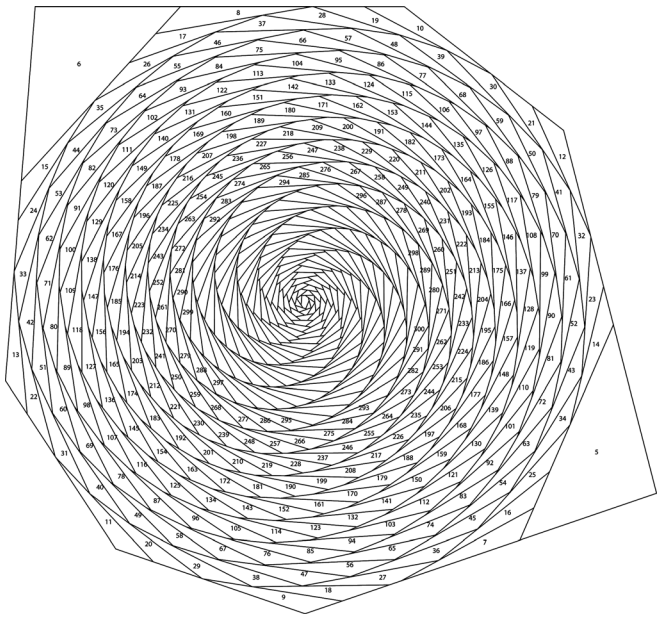

FIG. 13. Enlarged view of the central part of the forward spiral, with slices numbered according to the lengths of their respective flights.

area of the accelerator-mode island $\mathcal{A}_0^{(t)}$ of the local map with parameters g and h, the latter being given by Eq. (22) with $n = n(t) = n_0 + t$. The radius r_0 of this island is given by Eq. (30), and so we obtain for the area

$$|\mathcal{A}_0^{(t)}| = \frac{\pi}{4}\left(|n_0 + t|a\epsilon - g^2\right)^2. \tag{33}$$

The ratio of the two areas for our chosen parameters is plotted in Figure 14(b). The data show that that the expression (33) gives a rather accurate estimate of the measure of the flights, as long as the region $\Xi^{(t)}$ is not too small.

As N increases, the features of $\mathcal{W}$ become smoother. As the radial dimension of the tiles decreases, the tangential one converges to a value that depends only on the radial coordinate. Thus the tiles become segments, orthogonal to a radius passing through their centre, while the end-points of the segments arrange themselves along smooth spirals. The distortion appearing for large t are now confined to a decreasing region near the centre of $\mathcal{A}$.

The flights generated by the mechanism described above only tell half of the story. Just as the accelerator modes and their islands in the local model can be traced back to arbitrarily large negative times, the flights which accompany them (or in the PC case, replace them) can also be followed into the past using the restricted time-reversal involution H' introduced in Sec. III B.

By periodicity, it is sufficient to consider the flights which remain in the central H-atom, $\Psi^{(0)}$. The flights of interest all start in the domain $\Delta^{(n0)}$. Although for large N this polygon is approximately triangular (see Figure 12), it is in fact an H'-symmetric quadrilateral, with the reflection axis passing through the vertices $(-1/\varepsilon, 1)$ and $(-b/2, 0)$.

Consider now a flight originating at a point $z \in \Delta^{(n_0)}$. Let us suppose that the length of the flight is t, so that $z \in \mathcal{V}^{(t)} = L_{\rm pc}^{-t}(\mathcal{W}^{(t)})$. In order to keep matters simple, we assume that z is an interior point of that slice. Applying H' on z produces a mirror-image point z' located in $V^{(t')}$. Unless z happens to lie on the reflection axis, the points z and z' will be distinct, and unless the original slice happens to straddle the reflection axis, the flight time t' will not coincide with t. Thanks to the restricted time-reversal symmetry of Lemma 1, the length- t forward flight originating at z with be the H' reflection of the incoming flight arriving at z', while the length-t' forward orbit of z' is the mirror image of the incoming flight arriving at z.

Thus, apart from possible exceptions on the discontinuity set, knowledge of the forward portions of all the flights passing through $\Delta^{(n_0)}$ gives complete information about their histories for negative times. The latter can be summarized in a spiral diagram analogous to Figure 13. The numbered slices for arriving flights will just be the H' mirror images of their forward counterparts about the nearly vertical reflection axis. If the latter is plotted on the same diagram, it is seen to pass (apparently) through the center of the spiral.

D. Flight generation for the original map

We now return to our original dynamical system, the return map L induced on the region Λ by the piecewise isometry F given in Eq. (1). We wish to explore whether the mechanism for flight generation found for $L_{\rm pc}$ in the periodic chain model accurately portrays that found empirically for L. For the latter, we will restrict ourselves to the parameter range assumed in Ref. 17, namely

$$1 \le m < \lambda^{-1/4}, \quad 0 < \lambda \le 10^{-4}.$$

In this parameter range, the topology of the map L is consistent with that of the kite chain described in Sec. III. For fixed m, we satisfy ourselves with perturbative expressions (formal power series in λ, for given m and $\tau = \tan^{-1}(\Pi/4 \ -2n$

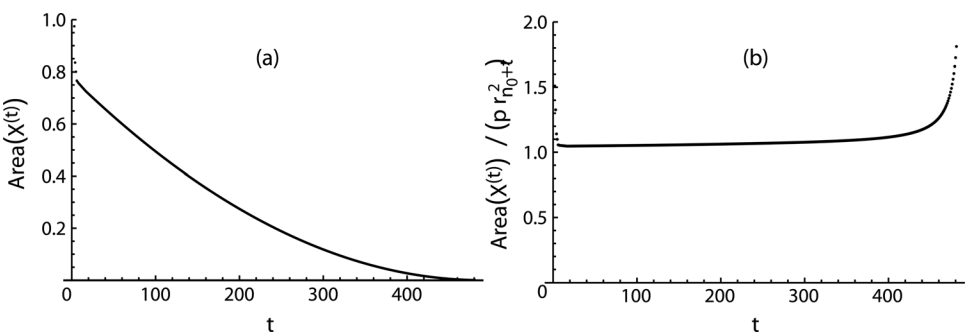

FIG. 14. (a) Decay of the area of $\Xi^{(t)}$ as a function of the flight time t, for the periodic chain model. (b) Plot versus t of the ratio of the area of $\Xi^{(t)}$ to that of the corresponding local accelerator-mode island $\mathcal{A}_0^{(t)}$, given by Eq. (33).

$\sin^{-1}(\lambda/2)$), without deriving explicit bounds on the Taylor remainders. As in Secs. IV A–IV C, we restrict ourselves to maximal-velocity, right-moving flights. This means that the parameter n will be assuming the role of $-n$ in the PC model, and the roles of the atom indices $i=0, 1$ will be interchanged correspondingly.

In order to make the comparison with the results for $L_{\rm pc}$ (and even $L_{\rm loc}$), we will need to define suitable quantities g and h as functions of m and τ. We choose as the "centre" w of $\Pi^{(n)}$ the midpoint of the G-symmetry line connecting $Q_0(n-1)$ to $Q_1(n)$:

$$w=\frac{1}{2}(Q_0(n-1)+Q_1(n)).$$

In order to compare with the PC and local coordinates, we rescale by a factor α which reduces the vertical separation between the centre and the upper boundary to unity, namely

$$\alpha^{-1}=1-w_y=\frac{\tau}{2}\lambda-\left(\frac{1+2\tau+5\tau^2}{8}\right)\lambda^2+\left(\frac{2+11\tau+10\tau^2+25\tau^3}{32}\lambda^3\right)+O(\lambda^4).$$

We can now determine g as a function of τ, and the inverse formula, by equating the rescaled distance between the two vertices of $\Pi^{(n)}$ on $y=1$ and the analogous PC quantity, $a=g+g^{-1}$:

$$g+g^{-1}=\alpha(Q_0(n-1)_x-Q_0(n)_x).$$

After some algebra, this gives

$$g=\tau-\frac{1+8\tau^2+7\tau^4}{4(1-\tau^2)}\lambda+\frac{19\tau+60\tau^3+126\tau^5+68\tau^7-17\tau^9}{16(1-\tau^2)^3}\lambda^2+O(\lambda^3),$$

$$\tau=g+\frac{1+8g^2+7g^4}{4(1-g^2)}\lambda-\frac{g-113g^3-98g^5+194g^7-81g^{11}}{16(1-g^2)^4}\lambda^2+O(\lambda^3).$$

We define the parameter h to be the vertical displacement of the line connecting $P_0(m)$ and $P_1(m)$ from the centre. A straightforward calculation yields

$$h=\tau^{-1}-2m+\frac{1+2\tau+5\tau^2-4\tau^3-8m\tau^3}{4\tau^2}\lambda+\frac{1}{48\tau^3}(3+6\tau+81\tau^2+144m\tau^2+48m^2\tau^2+42\tau^3-88m\tau^3-288m^2\tau^3-128m^3\tau^3-36\tau^5-72m\tau^5)\lambda^2+O(\lambda^3).$$

As in the PC model, we consider the flights initiated in the triangle

$$\Xi^{(0)}=\Delta_1^{(n)}=L(\Pi_1^{(n+1)})\cap\Pi_1^{(n)},$$

where n is less than the maximum value n_0 for a given m, namely the value such that

$$Q_0(n_0)<P_0(m)<Q_0(n_0-1),$$

and greater than a certain lower bound to be determined below. Flights of increasing length are generated by iterative application of L followed by intersection with the neighbouring atom:

$$\Xi^{(t)}=L(\Xi^{(t-1)})\cap\Pi_1^{(n+t)}.$$

Again these domains are bounded by the second-order intertwining polygons,

$$\Sigma_1^{(n)}=L(\Delta_1^{(n+1)})\cap\Pi_1^{(n)}.$$

For n sufficiently close to n_0 these are quadrilaterals, changing to triangles when one of the vertices of $L(\Delta_1^{(n+1)})$ crosses the line connecting $Q_0(n)$ to $Q_1(n)$. The crossing occurs at the solutions of the following equation:

$$0=3-\tau-6m\tau-\tau^2-5\tau^3+2m\tau^3+\frac{\lambda}{4\tau}(5-2m+4\tau+18m\tau+4m^2\tau+18\tau^2+40m\tau^2+74\tau^3+32m\tau^3-32m^2\tau^3+21\tau^4-6m\tau^4+70\tau^5-18m\tau^5-4m^2\tau^5).$$

Re-expressed in terms of g and h, the condition for this to happen is

$$h=\frac{1+5g^2}{3-g^2}-\frac{l(g)}{g^2(3-g^2)^3(1-g^2)}\lambda+O(\lambda^2),$$

where

$$l(g)=24+16g+25g^2+82g^3-74g^4-372g^5+36g^6-88g^7-14g^8+100g^9+3g^{10}+6g^{11}.$$

Note the lowest-order agreement with the PC-model result (29).

As n decreases further, the triangle eventually shrinks to a point, and this marks the upper bound on the length of flights in this family. The bifurcation value h_* is attained when the single vertex of $L(\Delta_1^{(n+1)})$ in $\Pi_1^{(n)}$ reaches the boundary line connecting $Q_0(n)$ to $Q_1(n)$. This is found to occur at the vanishing of

$$0=1-2m\tau-\tau^3+\frac{\lambda}{4\tau}(2+6m\tau+2\tau^2+12m\tau^2+13\tau^3+18m\tau^3-8m^2\tau^3+2\tau^4+13\tau^5+4m\tau^5)+O(\lambda^2),$$

or, in terms of g and h,

$$h=g^2+\frac{2+g+3g^2+5g^3-4g^4-15g^5-g^6-9g^7+2g^9}{2g^2(1-g^2)}\times\lambda+O(\lambda^2).$$

Again we have lowest-order agreement with the PC result, (29).

For sufficiently small λ, say $\lambda\le 10^{-4}$, the lowest-order terms in above formulae allow us to calculate fairly accurately the lengths of the longest flights for $m=1,2,\ldots$. In

TABLE I. Lowest-order estimates for the maximum flight lengths for $m=1,2,\ldots,10$. The lengths are expressed both in terms of the $O(\lambda^{-1})$ decrease in n (second column) and the $O(\lambda^0)$ horizontal displacement from start to finish (third column). The latter are computed by taking the differences of the x-coordinates of corresponding vertices of $\Pi^{(n_*)}$ and $\Pi^{(n_0)}$.

m	$(n_0-n_*)\times(10^4\lambda)$	$Q_0(n_*)-Q_0(n_0)$
1	1039.25	0.0600322
2	440.658	0.0231331
3	225.11	0.0115242
4	134.588	0.00682308
5	89.1005	0.0044956
6	63.2153	0.00318106
7	47.1343	0.00236795
8	36.4780	0.00183061
9	29.0595	0.00145723
10	23.6906	0.00118735

particular, the forward flights originate at $n=n_0$ and terminate at $n=n_*$, where

$$n_0\lambda \approx \frac{\pi}{4} - \tan^{-1}\frac{1}{2m+1}, \quad n_*\lambda \approx \frac{\pi}{4} - \tan^{-1}\frac{1}{2m+\tau_*^2},$$

where τ_* is the real solution of the cubic equation

$$\tau^3 + 2m\tau - 1 = 0.$$

The results for $m \le 10$ are listed in Table I.

A significant departure from the PC model (in addition to the obvious lack of periodicity with respect to the parameter m), is the continuous increase of g as a function of τ, for fixed m. This reflects itself in a variation in rotation number for the map L as one proceeds from $n=n_0$ to $n=n_*$. This can be seen in the tessellation of $\Xi^{(0)}$ generated by the flight-generating process in the spiral on the left in Figure 15. Careful examination of the picture allows one to see that the rotation angle, as a function of flight length, increases more rapidly as one spirals inward. In contrast, in the PC model, the rate of increase appears to be uniform (see Fig. 13).

Another difference between the two models is quite apparent in Figure 15, namely the assymmetry in the original model between forward and backward flights from points in the spiral of maximal size. In the PC model, in contrast, we have an additional time-reversal symmetry, H', which leads to the forward and backward spirals being mirror images of one another. In the original model, the symmetry is absent and this can easily be seen in the disparity between the lengths of the forward and backward flights originating at mirror-image points. For the parameters of figure, the forward flights are longer by an average ratio of approximately 4:3.

E. Local trapping and the turnaround phenomenon

The main emphasis of the present investigation has been to understand how long flights are created and sustained by the adiabatic destruction of accelerator-mode islands. The next step, which is beyond the scope of this work, is to understand in detail the post-flight behaviour. Here we merely set the stage by describing some of the preliminary empirical results and introducing some of the main issues which need to be addressed.

Perhaps the most prominent features of orbits involving flights are *local trapping* and the *turnaround phenomenon*. Once an orbit abandons a long flight, its fate is found empirically to be largely determined by the local map acting in a relatively short sequence of domains $\Pi^{(n)}$, often over a number of iterations comparable to the duration of the original flight. This is what we mean by local trapping (see Figure 4 for an example), and it stands in contrast to the diffusive wandering one finds for post-flight behaviour in chaotic models.[18–20] Eventually, the local motion lands in the vicinity of an accelerator mode and one has the possibility of jumping onto another long flight. The direction and velocity of the latter will depend on the identity of the accelerator mode, but, at least for the maximal-velocity flights emphasised in this article, the most likely outcome (by far) is a turnaround, i.e., a time-reversal of the original flight. This provides a considerable enhancement, via a double-turnaround scenario, in the probability of finding periodic orbits with relatively large stability disks and relatively short periods.

To illustrate the turnaround phenomenon, we considered the example of Figure 15, namely $\lambda=10^{-4}$, $m=3$, $i=1$, and $n=6434$. We chose a slice $V^{(106)}$, midway into the spiral, and calculated the partition corresponding to first return to $\Pi_1^{(6434)}$. We found that after 1000 iterations of L, there were 401 different domains which had returned to the original atom, all via the scenario of local trapping and turnaround. Most of

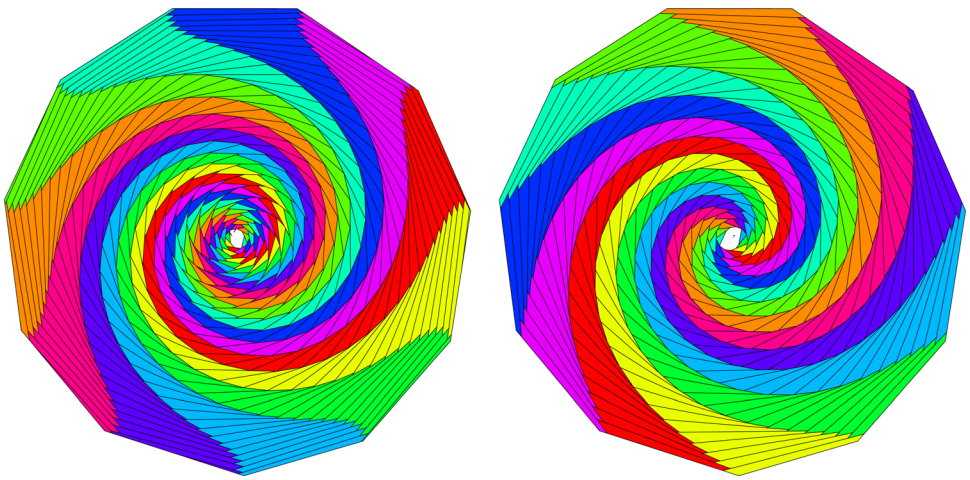

FIG. 15. (Color online) Tessellation of $\Xi^{(0)}$ produced by the flight-generation processes for L (on the left) and L^{-1} (on the right). In contrast to the forward spiral of the PC model (Figure 13) and its mirror-image backward partner, these spirals show evidence of the variation with n of the rotation number, as well as the asymmetry in flight length between forward and backward flights from mirror-image points.

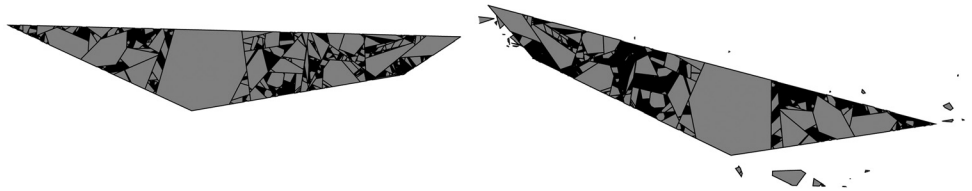

(a) (b)

FIG. 16. (a) First-return (to $\Pi_1^{(6434)}$) partition of $V^{(106)}$. The domains which have returned after 1000 iterations or less are shown in grey. Their return-map images, located in the G-reflected spiral, are shown in (b).

these ended up in the mirror-image spiral $G(\Xi^{(0)})$, in the slice $G(V^{(106)})$. This remarkable reconstitution of the slice in the G-symmetric location, brought about by numerous domains with different return paths and return times, is shown in Figure 16.

To test for periodic orbits and their islands, we calculated the first-return partition of the largest returning fragment in Figure 16, with a bound of 1200 iterations on the return time. Figure 17(a) shows the four cases with periods less than or equal to 1200. The largest island, occupying a significant fraction of the total area, has a period of 388. Its orbit, shown in Figure 17(b), consists of a G-symmetric pair of long flights, punctuated by short trapping episodes (10 iterations at $n = 6329$ and 12 iterations at $n = 6513$).

We are not yet in a position to offer a thoroughly convincing explanation of the turnaround phenomenon. However, it appears likely that it is closely related to the dominant role played by time-reversal symmetric orbits in the phase space. Consider the slice $W^{(t)}$ which leaves the flight path at step t. It is likely that most of the area of $W^{(t)}$ is covered by the islands of symmetric periodic orbits of $L_{\rm loc}$ which eventually find their way to the mirror-image region, $G(W^{(t)})$, and then get aboard a return flight which retraces the path of the original one. This could be the main ingredient of turnarounds, but obviously much more work is required to fully understand what is going on.

ACKNOWLEDGMENTS

This work was made possible by the Royal Society travel Grant No. TG091518.

APPENDIX: SOME FORMULAE

1. Local map: Atoms

We provide formulae for the atoms $\Pi_{i,k}$ of $\overline{L}_{\rm loc}$ as a list of vertices, ordered clockwise, with explicit parameter dependence,

$$\Pi_{1,1} = \left[\left(\frac{-g+g^3+2gh}{1+g^2}, \frac{-g^2(-2+h)+h}{1+g^2}\right), \left(\frac{-1+h+g^2(1+h)}{2g}, 1\right), \left(\frac{-1+h+g^2(3+h))}{4g}, 1\right)\right],$$

$$\Pi_{1,-1} = \left[\left(\frac{3+g^2(-1+h)+h}{4g}, -1\right), \left(\frac{1-2g^2(-2+h)+g^4(-1+h)+h}{2(g+g^3)}, \frac{g^2(-2+h)-h}{1+g^2}\right), \left(\frac{1}{g}, -1\right)\right],$$

$$\Pi_{1,0} = \left[\left(\frac{1+g^2(-1+h)+h}{2g}, -1\right), \left(\frac{-g+g^3+2gh}{1+g^2}, \frac{-g^2(-2+h)+h}{1+g^2}\right), \left(\frac{-1+h+g^2(3+h)}{4g}, 1\right), (g,1),\right.$$
$$\left. \times \left(\frac{1-2g^2(-2+h)+g^4(-1+h)+h}{2(g+g^3)}, \frac{g^2(-2+h)-h}{1+g^2}\right), \left(\frac{3+g^2(-1+h)+h}{4g}, -1\right)\right],$$

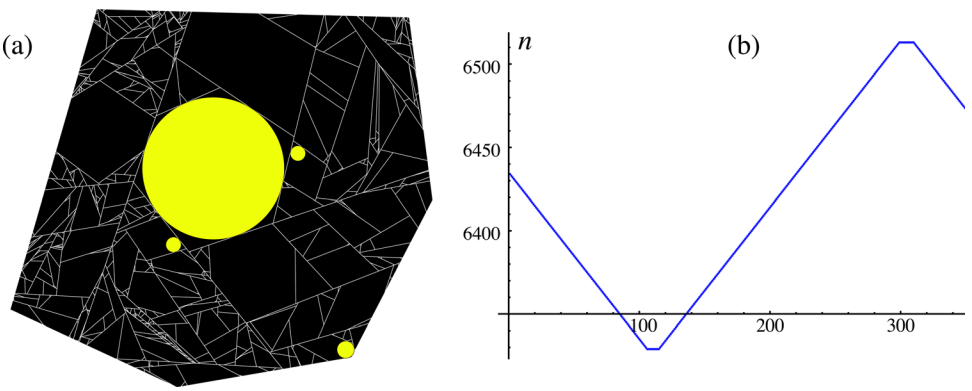

FIG. 17. (Color online) (a) First-return partition of the largest domain in Figure 16, showing the four islands associated with periodic orbits of period less than 1200. The n versus t itinerary of the period-388 island (the largest one) is plotted in (b).

$$\Pi_{0,1} = \left[\left(\frac{-1+h+g^4(1+h)-2g^2(2+h)}{2(g+g^3)}, \frac{-h+g^2(2+h)}{1+g^2}\right), \left(-\frac{1}{g}, 1\right), \left(\frac{-3+h+g^2(1+h)}{4g}, 1\right)\right],$$

$$\Pi_{0,-1} = \left[\left(\frac{1+g^2(-3+h)+h}{4g}, -1\right), \left(\frac{g-g^3+2gh}{1+g^2}, \frac{h-g^2(2+h)}{1+g^2}\right), \left(\frac{1+g^2(-1+h)+h}{2g}, -1\right)\right],$$

$$\begin{aligned}\Pi_{0,0} = \Bigg[&(-g,-1), \left(\frac{-1+h+g^4(1+h)-2g^2(2+h)}{2(g+g^3)}, \frac{-h+g^2(2+h)}{1+g^2}\right), \left(\frac{-3+h+g^2(1+h)}{4g}, 1\right),\\ &\times \left(\frac{-1+h+g^2(1+h)}{2g}, 1\right), \left(\frac{g-g^3+2gh}{1+g^2}, \frac{h-g^2(2+h)}{1+g^2}\right), \left(\frac{1+g^2(-3+h)+h}{4g}, -1\right)\Bigg].\end{aligned}$$

2. Local map: Triangle Δ

We list the vertices $\Delta_{i,j}$ of the triangle $\Delta = \Delta_0$.

$$\Delta_{1,2} = \left[-\frac{1+g^2+h-g^2h}{2g}, h\right],$$

$$\Delta_{2,3} = \left[-\frac{1+g^2-3g^2h+g^4h}{2g(1-g^2)}, h\right],$$

$$\Delta_{1,3} = \left[\frac{-1+h+g^4(1+h)-2g^2(2+h)}{2g(1+g^2)}, \frac{-h+g^2(2+h)}{1+g^2}\right].$$

3. Periodic chain map: Atoms

We provide formulae for the atoms $\Pi_i^{(n)}$ of $L_{\rm pc}$ as a list of vertices, ordered clockwise.

$$\Pi_0^{(n)} = \begin{cases} [Q_0(n-1), R_1(n), R_0(n), Q_1(n), Q_1(n-1)] & \text{if } (\mathrm{n}+(\mathrm{N}-1)/2) \equiv 0 (\mathrm{mod}\, N) \\ [Q_1(n-1), R_1(n), R_0(n)] & \text{if } (n-(N-1)/2) \equiv 0 (\mathrm{mod}\, N) \\ [Q_0(n-1), R_1(n), R_0(n), Q_1(n-1)] & \text{otherwise} \end{cases} \tag{34}$$

$$\Pi_1^{(n)} = \begin{cases} [Q_0(n), R_0(n), R_1(n)] & \text{if } \mathrm{n}+(\mathrm{N}-1)/2 \equiv 0 (\mathrm{mod}\, N) \\ [Q_0(n), Q_1(n), R_0(n), R_1(n), Q_0(n-1)] & \text{if } \mathrm{n}-(\mathrm{N}-1)/2 \equiv 0 (\mathrm{mod}\, N)\,, \\ [Q_0(n), Q_1(n), R_0(n), R_1(n)] & \text{otherwise} \end{cases}$$

where

$$Q_0(n) = (g+na, 1), \quad Q_1(n) = (1/g+na, -1),$$
$$R_0(n) = G(R_0'(n)), \quad R_1(n) = G(R_1'(n)).$$

The quantities $R_{1,2}'$ are defined as follows. If $n+(N-1)/2 \equiv 0 \pmod N$, then $R_0'(n) = (m(n)b - 1/\epsilon, 1)$; otherwise R_0' is the intersection of two segments, given by

$$\{R_0'(n)\} = [Q_0(n-1), Q_1(n-1)] \cap [(m(n)b - 1/\epsilon, 1), (m(n)b + 1/\epsilon, -1)].$$

Likewise, if $n-(N-1)/2 \equiv 0 (\mathrm{mod}\ N)$, then $R_1'(n) = (m(n)b + 1/\epsilon, -1)$; otherwise

$$\{R_1'(n)\} = [Q_0(n), Q_1(n)] \cap [(m(n)b - 1/\epsilon, 1), (m(n)b + 1/\epsilon, -1)].$$

4. Periodic chain map: Triangle Δ

We list the vertices $\Delta_{i,j}$ of the triangle Δ for the periodic chain map. Let $\Theta = \sqrt{1+\epsilon^2}$. We have

$$\Delta_{1,2} = \left[\frac{\epsilon + \epsilon g^2 + 2gh}{\epsilon(\epsilon - 2g - \epsilon g^2)}, \frac{\epsilon + \epsilon g^2 + 2gh}{2g + \epsilon(-1 + g^2)}\right],$$

$$\begin{aligned}\Delta_{2,3} = [&(-\epsilon\Theta - g - \epsilon^2 g + \Theta g - \epsilon\Theta g^2 - g^3 - \epsilon^2 g^3 + \Theta g^3 \\ &+ \epsilon h - 3gh + \Theta gh - 3\epsilon g^2 h + g^3 h + \Theta g^3 h)/(\epsilon(-\epsilon \\ &+ 2g - 2\epsilon^2 g + 6\epsilon g^2 - 2g^3 + 2\epsilon^2 g^3 - \epsilon g^4)), \\ &(-\epsilon\Theta - g - \epsilon^2 g + \Theta g - \epsilon\Theta g^2 - g^3 - \epsilon^2 g^3 + \Theta g^3 \\ &+ \epsilon h - 3gh + \Theta gh - 3\epsilon g^2 h + g^3 h + \Theta g^3 h)/ \\ &(\epsilon - 2g + 2\epsilon^2 g - 6\epsilon g^2 + 2g^3 - 2\epsilon^2 g^3 + \epsilon g^4)],\end{aligned}$$

$$\begin{aligned}\Delta_{1,3} = [&(\epsilon - 2\epsilon\Theta - 2g + 2\epsilon^2 g + 2\Theta g - 6\epsilon g^2 + 2\epsilon\Theta g^2 \\ &+ 2g^3 - 2\epsilon^2 g^3 - 2\Theta g^3 + \epsilon g^4 + 2\epsilon h - 4gh \\ &+ 2\Theta gh - 2\epsilon g^2 h - 2\Theta g^3 h)/(\epsilon(1 + g^2)(-\epsilon + 2g \\ &+ \epsilon g^2)), (\epsilon^2 - 4\epsilon g + 4e\Theta g + 4g^2 - 2\epsilon^2 g^2 \\ &- 4\Theta g^2 + 4\epsilon g^3 + \epsilon^2 g^4 - 2\epsilon gh + 4g^2 h - 4\Theta g^2 h \\ &+ 2\epsilon g^3 h)/(\epsilon(1 + g^2)(-\epsilon + 2g + \epsilon g^2))].\end{aligned}$$

[1]Adler, R., Kitchens, B., and Tresser, C., "Dynamics of nonergodic piecewise affine maps of the torus," Ergod. Theory Dyn. Syst. **21**, 959–999 (2001).
[2]Ashwin, P., "Elliptic behaviour in the sawtooth standard map," Phys. Lett. A **232**, 409–416 (1997).
[3]Avila, A., and Forni, G., "Weak mixing for interval exchange transformations and translation flows," Ann. Math. **165**, 637–664 (2007).
[4]Bunimovich, L. A., and Dettmann, C. P., "Open circular billiards and the Riemann hypothesis," Phys. Rev. Lett. **94**, 100201 (2005).
[5]Buzzi, J., "Piecewise isometries have zero topological entropy," Ergod. Theory Dyn. Syst. **21**, 1371–1377 (2001).
[6]Chirikov, B., "A universal instability of many-dimensional oscillator systems," Phys. Rep. **52**, 263–379 (1979).
[7]Chirikov, B., "Time-dependent quantum systems", in *Chaos and Quantum Physics*, edited by M. Giannoni, A. Voros, and J. Zinn-Justin, (North-Holland, 1991) p. 443.
[8]Chua, L. O., and Lin, T., "Chaos in digital filters," IEEE Trans. Circuits Syst. **CAS-35**, 648–658 (1988).
[9]Dana, I., "Global superdiffusion of weak chaos," Phys. Rev. E **69**, 016212 (2004).
[10]Goetz, A., "Dynamics of piecewise isometries," PhD Thesis (University of Chicago, 1996).
[11]Goetz, A., and Quas, A., "Global properties of a family of piecewise isometries," Ergod. Theory Dyn. Syst. **29**, 545–568 (2009).
[12]Gutkin, E., and Haydn, N., "Topological entropy of polygon exchange transformations and polygonal billiards," Ergod. Theory Dyn. Syst. **17**, 849–867 (1997).
[13]Hooper, W. P., "Renormalization of polygon exchange maps arising from corner percolation," preprint (2011), e-print arXiv:1105.6137v2, 47 pages.
[14]Kouptsov, K. L., Lowenstein, J. H., and Vivaldi, F., "Quadratic rational rotations of the torus and dual lattice maps," Nonlinearity **15**, 1795–1842 (2002).
[15]Lamb, J. S. W., and Roberts, J. A G., "Time-reversal symmetry in dynamical systems: A survey," Physica D **112**, 1–39 (1998).
[16]Lowenstein, J. H., Poggiaspalla, G., and Vivaldi, F., "Sticky orbits in a kicked oscillator model," Dyn. Syst. **20**, 413–451 (2005).
[17]Lowenstein, J. H., and Vivaldi, F., "Approach to a rational rotation number in a piecewise isometric system," Nonlinearity **23**, 2677–2721 (2010).
[18]Zaslavsky, G. M., and Edelman, M., "Maxwell's demon as a dynamical model," Phys. Rev. E **56**, 5310–5320 (1997).
[19]Zaslavsky, G. M., Edelman, M., and Niyazov, B. A., "Self-similarity, renormalization, and phase space nonuniformity of Hamiltonian chaotic dynamics," Chaos **7**, 159–181 (1997).
[20]Zaslavsky, G. M., and Niyazov, B. A., "Fractional kinetics and accelerator modes," Phys. Rep. **283**, 73–93 (1997).